Construction and validation of a low cost paediatric pelvis phantom

Mr. Ali Mohammed Ali[1]

Professor Peter Hogg[1]

Dr. Safora Johansen[2]

Dr. Andrew England[1]

[1]School of Health Sciences, University of Salford, Salford M6 6PU, United Kingdom.

[2]Oslo Metropolitan University, Faculty of Health Sciences, Norway.
[2] Department of Oncology, Division of Cancer Medicine, Surgery and Transplantation, Oslo University Hospital, Radiumhospitalet, Oslo, Norway.

Corresponding author:

Mohammed Ali, A

Phone number: +447442541734

Email: a.h.m.a.mohammedali@edu.salford.ac.uk

Authors:

Professor Hogg, P   Email: P.Hogg@salford.ac.uk

Dr. Johansen, S   Email: saferajo@oslomet.no

Dr. England, A   Email: A.England@salford.ac.uk

ABSTRACT

PURPOSE: Imaging phantoms can be cost prohibitive, therefore a need exists to produce low cost alternatives which are fit for purpose. This paper describes the development and validation of a low cost paediatric pelvis phantom based on the anatomy of a 5-year-old child.

METHODS: Tissue equivalent materials representing paediatric bone (Plaster of Paris; PoP) and soft tissue (Poly methyl methacrylate; PMMA) were used. PMMA was machined to match the bony anatomy identified from a CT scan of a 5-year-old child and cavities were created for infusing the PoP. Phantom validation comprised physical and visual measures. Physical included CT density comparison between a CT scan of a 5-year old child and the phantom *and* Signal to Noise Ratio (SNR) comparative analysis of anteroposterior phantom X-ray images against a commercial anthropomorphic phantom. Visual analysis using a psychometric image quality scale (face validity).

RESULTS: CT density, the percentage difference between cortical bone, soft tissue and their equivalent tissue substitutes were -4.7 to -4.1% and -23.4%, respectively. For SNR, (mAs response) there was a strong positive correlation between the two phantoms (r>0.95 for all kVps). For kVp response, there was a strong positive correlation between 1 and 8 mAs (r=0.85), this then decreased as mAs increased (r=-0.21 at 20 mAs). Psychometric scale results produced a Cronbach's Alpha of almost 0.8.

CONCLUSIONS: Physical and visual measures suggest our low-cost phantom has suitable anatomical characteristics for X-ray imaging. Our phantom could have utility in dose and image quality optimisation studies.

Keywords: Pelvis phantom, low-cost, dose optimisation, validation, development.

1- Introduction

Phantoms used in medical imaging are commonly divided into groups according to the purpose they serve, for example image quality (IQ) evaluation and radiation dosimetry [1]. Imaging phantoms typically comprise of physics-based test objects and anthropomorphic phantoms, the latter are generally more complex being designed to facilitate the assessment of IQ. Dosimetry phantoms are used for estimating the radiation dose received by patients when undergoing medical imaging procedures or radiotherapy treatments [2,3]. Access to anthropomorphic phantoms with sufficient replication of body tissues, composition, size and shape is not always possible. Reasons for this include the relative complexities of phantom manufacture, lack of availability and the high overall cost. More simpler geometrical phantoms have, therefore, been designed to provide options for dosimetry and IQ evaluation [4,5] but these have limitations. Phantoms routinely used in IQ assessments are not generally customisable according to a patient's age, gender or stature. Dosimetry phantoms are, however, more likely to display size and gender variations but are often restricted in their availability and are usually not suitable for IQ evaluations [1]. It has been reported [6] that the simulation of the human body from the newborn to adult, for radiographic examinations, is challenging. Huge discrepancies exist in the dimensions and tissue densities within the human body. This problem is further confounded in paediatrics where there are more marked size and density variations as the child develops [7].

Designing and constructing a phantom for X-ray imaging requires careful consideration of a number of criteria. Firstly, the selection of materials (tissue substitutes) that provide a similar response to radiation exposure, at specific energies, needs to replicate human tissue as closely as possible. Second, is the ability of those tissue substitutes to physically form the internal and external components of the human body [6,8]. Third, a further complexity in pelvic imaging is providing a representative interface between bone and soft tissue, which is necessary for successful image interpretation [9]. Finally, size variations are important in phantom design, the bulk of the commercially available phantoms are based on the morphology of either neonates or adults. Phantoms representing child ages between 1 and 15 years are urgently needed.

Previous studies[10–13] have considered the average bone density for cortical and trabecular layers of bone. Other studies have used aluminium as a material in order to simulate bone [4,5,14–16]. However, these studies produced phantoms which lacked the geometrical representation necessary for IQ evaluation studies. A number of phantom development studies [17,18] focused specifically on dosimetry and the accuracy of the anatomical representation was not considered with density being averaged between cortical and trabecular bone. Other phantoms did not include bone in their construction [19], whereas others [20–22] used one single material to simulate the whole human body.

When undertaking imaging research, largely due to ethical issues, the evaluation of visual IQ typically involves images generated from phantoms [5]. Additionally, many authors have demonstrated that physical measures of IQ are insufficient on their own to investigate the clinical benefit of one imaging technique over another [9].

The aim of our work was to develop and validate a low-cost dosimetry / IQ pelvic phantom, based on the dimensions and tissue characteristics of a 5-year-old child and to determine whether it is appropriate for optimisation studies.

2- Materials and methods

The pelvic area of the human body is geometrically complicated in terms of its bony components such as the iliac crest, pubis, sacrum and the femur. Each component is shaped in a manner where its thickness varies along with its dimensions. To simulate each bony component accurately, the radiological characteristics and anatomical shape of the patient should be considered within the phantom design. As a result, the phantom should have a precise human anatomical shape, matching dimensions and be constructed from the correct tissue substitutes [3,6,8]. In order to provide accurate replicas of bony pelvic structures, our phantom was constructed using CT data acquired from a 5-year-old child. Once the dimensions of the bony pelvis components were available a process was introduced for selecting appropriate tissue substitutes, finally a series of validity tests were performed to assess the functionality of the newly constructed phantom. With the majority of clinical indications for pelvis radiography being based around the identification or exclusion of bony pathology, the construction of the phantom focused on bony and soft tissue components. Soft tissue components, including blood vessels, muscles and adipose tissue, were likely to have similar X-ray characteristics and as such were designed to be manufactured from a single material. Our study was quantitative in design, with the intention of validating the phantom for use in radiographic optimisation studies.

2.1- Phantom manufacturing procedure

2.1.1- Material selection

The level of agreement between the selected tissue substitute and actual human tissue is dependent on the requirements of the phantom. Generally, tissue substitutes for X-ray imaging modalities do not need to be matched for all types of radiation interactions [8]. Furthermore, in diagnostic X-ray applications it is only necessary to have a linear attenuation relationship within the specific clinical energy range (i.e. those generated by diagnostic X-ray equipment). Agreement with linear attenuation has already been established and consequently the radiation characteristics of a substitute should give a similar response to that of human tissue [2,23].

Theoretical matching of human tissues and potential tissue substitutes can be made by calculating attenuation coefficients [24]. Using this approach mass attenuation coefficients can be calculated after entering the compound proportions of any material using web-based software [25]. All tissues in the pelvic area are of comparable linear attenuation coefficients when compared to soft tissue, except for cortical bone (**Figure 1**). The percentage error for polyvinyl chloride (PVC) representing the cortical bone of 5-year-old child was determined. The results showed that the percentage difference in attenuation coefficients varied from 5.7% to 14.2% at 50 kV and 100 kV, respectively. For the PMMA, the percentage error from actual soft tissue ranged from 2.0% to 7.9% at 50 kV and 100 kV, respectively. PVC has been reported as a substitute for cortical bone (ICRU 44) [25]. PVC is, however, a solid material at room temperature and consequently there are difficulties when attempting to fill complex

spaces representing bony structures. Molten PVC generates toxic gases and it is not safe to use in standard laboratories without complex safety procedures. Plaster of Paris (PoP) has been reported as a potential alternative substitute and was selected as the cortical bone substitute as it is easily moulded into complex spaces and poses no health and safety threat. PMMA was used as the soft tissue equivalent [24,25] (**Figure 1).** PoP has been reported [25] as a possible cortical bone substitute and has been used in literature for imaging of paediatric distal extremities [26] and the construction of body contours [27]. The problem with this substitute is that its density does not exactly match that of paediatric cortical bone [28]. This is a potential source of error and could exclude this material from being a potential substitute. However, CT experimentation via density calculations revealed that different mixing ratios of the Plaster with water resulted in different densities of solidified PoP. These compounds were then evaluated, using CT, and the density of plaster was matched to the attenuation characteristics similar to cortical bone (**Figure 2**). Steps for matching the attenuation properties of the substitutes to patient data are described in the CT validation method.

2.1.2- Design of the phantom

Constructing a radiographic imaging phantom using dimensions obtained from axial CT data has been used successfully in dosimetry phantoms [10], but for imaging phantoms it would be likely to produce visual air gaps between the axial sections [29]. In order to overcome this problem, our phantom was constructed using CT images reconstructed in the coronal plane [17]. Reconstruction of CT images in the coronal plane was achieved using the computer software RadiAnt DICOM viewer (v 3.4.2.13370, Medixant, Poland). As mentioned previously, CT data from a patient provides realistic anatomy and measurements from this can provide accurate dimensions to be used in the construction of the phantom [17]. The overall body trunk dimensions (thickness, 12 cm; width, 22 cm; length, 25 cm) were taken from the same paediatric CT scan. Further to this, phantom design was carried out by templating the CT coronal images directly onto slabs of PMMA (the soft tissue substitute) and cutting them using a handheld milling tool. PMMA edges were smoothed by aligning different serial slices and using a smoothing tip on the milling machine and sanding the edges with glass paper. PMMA slices were 2 mm thick in order to maintain anatomical detail as thicker slices would produce a less representative shape of the bony components of the human pelvis. This resulted in PMMA slabs containing cavities from which the bony anatomical shapes could be created using infused liquid PoP (**Figure 3**).

Trabecular pattern and further cortical bone was included in the phantom via insertion of a cadaveric animal (chicken) bone. Animal bones have been used in literature to simulate parts of human body, such as the legs [30].

2.1.3- Assembling the phantom

To fill the phantom cavities with PoP a number of steps were needed. The correct proportions of water and PoP powder needed to be weighed using the ratios of 30 g and 50 g, respectively (**Figure 2**). Once mixed with water the PoP was ready for infusion into the PMMA slabs. After filling, the plaster surfaces were flattened for each PMMA block by wiping plaster surface as soon as it solidified, so that all the assembly of all blocks were flat and fitted together.

2.1.4- Timeline and costs

The phantom design and construction included the development of a prototype model and then the final design. The working hours for milling the phantom slices, joining them together and smoothing them out was approximately 20 hours. To cast the PoP into the PMMA this needed around 10 hours. The total effort for phantom construction was approximately 30 hours; this did not include any PoP drying out time (**Figure 2**). Total costs of the phantom construction, excluding labour was approximately £53.

2.2- Validation process

2.2.1- CT validation

CT numbers represent the X-ray attenuation characteristics of different materials, these are related to the density of the tissue or its substitute. Measured HU values from a CT scan are one of the methods reported in literature to identify and compare the density and composition of tissues and their substitutes [31,32]. The standard deviation (SD) from the CT based region of interests (ROIs) can also be used as an indication of the homogeneity of materials when compared to a valid tissue substitute [32].

A Toshiba Acquillion 16 CT scanner (Toshiba Medical Systems, Crawley, UK) was used for data acquisition. Parameters included 80 kVp, 100 mAs, detector configuration 1 mm x 16, rotation time 0.5 seconds, image slice thickness 1 mm and reconstruction interval 1 mm. CT acquisition parameters were selected to match those previously used to acquire clinical CT data used in the phantom construction.

Tests were then carried out to make sure that the PoP had similar attenuation characteristics to the cortical bone using the CT data from the 5-year-old child. This was achieved by finding the correct weight-mixing ratio between the plaster powder and water, using a scale with 0.001 g error. In order to test and identify the correct mix, five different weight-mixing ratios were prepared: 30/50, 34/50, 38/50 and 42/50 (water/PoP) ratio beside cadaveric animal bone. Using the RadiAnt DICOM viewer software, the percentage difference between the CT density for the phantom and the patient data were calculated.

2.2.2- Geometrical simulation from the CT data

CT scanning was also used to compare the dimensions of the phantom against the patient-based CT dataset. In the literature, CT data can be used to template phantom components with high precision. CT data from the phantom can also be used to compare dimensions of the patient-based CT dataset against those acquired from the newly constructed phantom. A three-dimensional (3D) reconstruction, using RadiAnt DICOM viewer, was constructed in order to visually evaluate the phantom geometry against the real patient CT data (**Figure 4**).

2.2.3- Pixel value validation

The determination of each pixel value is related to the attenuation of X-rays that pass through the corresponding body part [33]. The amount of information contained in a digital image is determined by number of pixels it contains, which represents the number of different intensities from each pixel [34]. One of the commonest approaches used to measure the overall information visibility on an image is the quantity signal to noise ratio (SNR). In digital radiography, a well-established description of image quality is SNR because, using the benefit

of image processing, the appearance of large low contrast details is limited only by noise [35]. SNR is a physical measure of image quality and is extensively used in optimisation studies [36].

An adult anthropomorphic pelvis phantom (RS-113T, RSD, Long Beach, CA) was used as a reference phantom for comparison against our newly manufactured 5-year-old pelvis phantom. The parameters set for comparing SNR from our 5-year-old representative phantom with the commercially available adult phantom is as follows: the tube potential used was 50 to 101 kVp rising in 3 KVp increments, the mAs range varied from 1 to 20, the SID was fixed at 110 cm and no grid was used. The collimation was set to 29 x 34 cm for the adult phantom and 24 x 20 cm for the 5-year-old phantom. Image post-processing was set to 'quality control test' in order to avoid any manipulation in the resultant pixel values. Overall tissue thickness (21 cm) was matched between the two phantoms to generate equivalent incident air kerma (IAK) values.

Measurements of SNR were taken from a total of 23 ROIs on the two phantom X-ray images (**Figure 5**). ImageJ software (v 1.49, NIH, US) was used for the physical measurements (SNR). A Pearson's correlation coefficient (r) was calculated as an indicator of the similarity in SNR responses between the two phantoms.

2.2.4- Face validation

A validated list of 15 questions were presented to observers and they were asked to evaluate the visual appearance of the resultant X-ray images generated from our 5-year old phantom. Each question related to the visibility of different parts of the pelvis. Fourteen questions related to the appearances of the pelvic anatomy and were derived from the psychometric image quality scale developed by Mraity et al. [37]. Questions (Q) included anatomy such as; Q1: hip joints, Q2: greater trochanters, Q3: lesser trochanters, Q4: iliac crests, Q5: pubic & ischial rami, Q6: proximal femora, Q7: sacro-iliac joints, Q8: femoral necks, Q9: sacrum and its inter-vertebral foramina, Q10: bone/soft tissue interface, Q11: body of L5, Q12: obturator foramina, Q13: acetabula and Q14: rotation and tilting. In addition, one question asked whether the phantom image would allow the assessment of IQ at different exposure factors. A 5-point Likert scale was used in the questionnaire and participants were asked to rate their agreement with the statements (strongly agree +2, agree +1, neither agree/disagree 0, disagree -1 and strongly disagree -2).

The questionnaire together with an X-ray image from the 5-year- old phantom were showed to 32 second year UK diagnostic radiography students. These observers were aware of the radiographic technique and had experience in X-ray image appraisal. The purpose of this phase of the study was to seek the perspectives from trained radiography students on the visibility of key anatomical features on the X-ray image from each phantom. Previously such studies [38,39] have used between 5 to 10 observers to evaluate image quality, so our sample size is quite large. In addition to the student observers, four experts with more than ten years experience (two radiologists and two qualified radiographers) were included in the evaluation of the phantom X-ray image. For the purposes of the face validation, the University Ethics Committee approved this component of the project (HSR1617-78).

Questionnaire responses from all participants were taken as mean values for each question (the answers for negatively-worded questions were taken as mean values then converted to positive score). If only a limited number of questionnaire items were positively scored in terms of being visible on the resultant phantom X-ray image these data would be used to propose a modified IQ scale which could be used with the newly developed phantom. If this occurred, then Cronbach's alpha would be calculated to estimate the internal consistency of the modified IQ scale.

2.3- Statistical analysis

The computer software SPSS Statistics v23 (IBM Inc, Armonk, NY) was used for data analysis. Mean values together with their respective standard deviations (SD) were reported for data that were approximately normally distributed. For non-parametric data median values together with the inter-quartile range were reported. Normality of the data were established using the Shapiro-Wilk test (a P value greater than 0.05 was considered to represent an approximately normal distribution). A Pearson's correlation coefficient was utilised for the comparison of mean pixel values for the adult and 5-year-old phantoms. As previously stated Cronbach's alpha would be used to calculate the internal consistency of any modified IQ scale.

3- Results

3.1- CT validation

The results comparing the CT density (HU) of PoP to that of human cortical bone (patient CT data) are shown in **Table 1**. A 30/50 (water/PoP) ratio gives the closest CT attenuation characteristics to cortical bone for 5-year-old patient, with a 2.5% difference between CT data from the patient human and test samples of PoP. Also, the CT data confirmed that the drying time for the PoP was approximately 7 days (**Figure 2**).

The average of CT density, for both PoP and cortical bone, was measured over each anatomical area. This calculation method allowed each anatomical component to have equal impact on the overall mean CT density for bone. This reference quantity from the patient's CT data was compared against the averaged CT density for PoP in the phantom (**Table 1**). The percentage difference between the averaged CT density of cortical bone and the PoP was <5% (**Table 1**).

The percentage difference in CT density between the PMMA and soft tissue was -23.4%. However, the percentage difference between cortical bone and soft tissue and their equivalent tissue substitutes in the phantom were 176.8% and 172.2%, respectively. The difference between the comparative human tissues and those in our phantom were 4.6%.

The results of the CT density evaluation of the animal bone (cortical) component of the phantom (**Table 1**), showed similar average HU values (1212.4) to human bone and the percentage difference to patient cortical bone was -1.0%. These low level differences provides further evidence of phantom validation.

3.2- CT homogeneity test

The SD from the CT based ROIs can be used as an indication of the homogeneity of materials when compared to a valid tissue substitute [32]. Evaluating the range of SD values for the PoP/animal bone and PMMA, when compared to cortical bone and soft tissue, respectively,

are reported in **Table 1**. Using the SD data, it appears that there is no substantial heterogeneity of the bone substitute used (-4% SD difference).

3.3- Pixel value validity

Correlation coefficients between the adult anthropomorphic phantom and our phantom representing a 5-year-old, with a calibrated thickness (21 cm), were acquired (**Table 2**). In terms of mAs response, there was a strong positive correlation between SNRs from the two phantoms (r>0.95 across all kVps). For kVp, there was a strong positive correlation between 1 to 8 mAs (average r>0.85 (averaged for the PoP and PMMA)), this then decreased as the mAs was increased (r=-0.21 at 20 mAs (averaged for PoP and PMMA)).

3.4- Face validity

Questionnaire responses were collected from all of the participants (n=32) and all answers were averaged for each question. The average score for the overall answers (Q1 to Q14) was 0.47, this indicated a tendency of the participants to agree with the statements regarding suitability of the paediatric pelvis phantom to generate realistic images of an AP pelvis projection. Beside Q15 with a score 0.84, data from this section of the experiment indicates that the participants favoured the general applicability of the phantom for visual image quality optimisation studies (**Table 3**).

Based on the questions which had high scores, seven questions were chosen to provide a modified IQ scale for the 5-year-old phantom. Questions selected where the average values (ranged from 0.53 to 0.88) and included Q1, Q5, Q7, Q8, Q9, Q11 and Q13 (**Table 3**). The questionnaire results, also, showed a highly positive agreement on the questions that formed the phantom IQ scale with high internal consistency (Cronbach's alpha = 0.8).

4- Discussion

4.1- CT validation

The CT density (HU) measurements from **Table 1** demonstrate the agreement between the phantom materials and the human tissues. These levels of agreement are related to the X-ray attenuation characteristics [40]. Percentage differences between tissues and their substitutes, such as cortical bone and PoP/animal bone, were recorded with values less than 5% (**Table 1**). Thus, according to the tissue classification system [2,25], PoP is a class A substitute and falls within an acceptable error rang of 5% [2,3,25].

The percentage difference in CT density between the PMMA and soft tissue was -23.4%. This percentage difference is unlikely to affect study results since there are many structures which make up the soft tissues, for example muscle which reaches 100 HU [31] and thus there are natural heterogeneities in soft tissues.

The percentage difference between cortical bone and soft tissue (patient) and PoP to PMMA (phantom) generated similar values (176.8% and 172.2%, respectively). The difference between the patient and phantom data was 4.6%. This relatively small difference would reflect similar visibility (contrast) of the bony anatomy alongside soft tissue (patient) when compared with PoP alongside PMMA (phantom) and provide further evidence of phantom validity. In

addition, the percentage difference between the patient and animal cortical bone was -1.0% again providing further evidence of phantom validation.

4.2- CT homogeneity test

The SD from **Table 1** demonstrated no considerable heterogeneity from the substitutes of the cortical bone and the soft tissues. While, the literature already reports a wide range of HU values from soft tissue including the fat and muscle [31] and as such demonstrates natural heterogeneities which occur in the human body and would be expected within a phantom of this intended purpose. Within our work this was demonstrated by the -23% difference in SD for the soft tissue structures.

4.3- Pixel value validity

The high correlation between the two phantoms can be explained by the high level of structural replication of the phantom and the production of the subsequent X-ray images. Such high correlations demonstrates validity against the adult anthropomorphic phantom.

4.4- Face validity

The results from face validity showed an average score of 0.47 (Q1 to Q14), this indicates a tendency of the participants to agree with the statements that the X-ray imaging characteristics of the phantom are representative of a paediatric AP pelvis projection.

The results for the validity of the IQ scale (0.8 Cronbach's alpha coefficient) relate to the radiographic properties that exist in the human pelvis, these are found within our phantom. The results appear to be reflective of a human based pelvis X-ray image. It is highly likely that the IQ subscale has valid performance for visual assessment of image quality. The high face validity also confirms the perception that the observers had on the high similarity of the geometry of the anatomies and their substitutes' x-ray characteristics, these must be a close match [3].

5- Limitations

Phantom manufacturing, in general, has many limitations in its procedures, this often leads to limited designs and representations of human structures. Firstly, the availability of the tissue substitutes and the formation of complex shapes which are needed to represent the human body. In addition, some materials are also subjected to industrial confidentiality and are not widely available [17,32]. Secondly, the complexity in the requirements for manufacturing systems that allow the preparation of phantom materials such as vacuum equipment [2], which would add extra difficulty in the geometrical formation of components is a potential problem. Those aforementioned limitations have made it necessary for this phantom to contain trabecular bone and additional anatomical details from the inclusion of an animal bone. However, this limitation is of limited effect when evaluating the edge of cortical bone against soft tissue, a task that does not require the presence of trabecular bone as is well simulated within the phantom. When measuring the estimated surface dose, by placing dosimeter on the phantom's surface, the phantom can also be successfully used in dose optimisation studies.

After going through the manufacturing process of this phantom, a series of improvements to the current phantom can be suggested. Improving the phantom productivity time by using thicker slices may be achieved by using 3D or improved milling technology. 3D printing is an

alternative technology that should also be considered as it can also offer greater replication of individual patient anatomy. New materials are constantly being developed and it is likely that printing filaments will have sufficient densities to replicate a wide range of human tissues and provide much wider phantom construction opportunities. Within the literature, there are reports of the potential role of 3D printing in phantom development and construction [41,42]. It is likely that at present such processes will be expensive and require access to technologies with limited availability. In many parts of the world, logistics and economics would restrict access to 3D printing and alternatives are required such our method of phantom construction.

6- Conclusion

A series of validation experiments were carried out in order to investigate whether our phantom is capable of generating images for radiographic optimisation studies. From the CT validation work, density measurements showed percentage difference in the contrast between the patient and the phantom in the range of 4.6% (176.8% - 172.2%). Percentage differences between the materials in the phantom and the tissues in the patient were also similar (**Table 1**). These differences mean that the phantom materials would simulate the radiological properties of a human pelvis of the corresponding age. Pixel validation also showed a strong correlation (r>0.85) with the phantom X-ray images, at different exposure factors. Our phantom delivered similar responses in terms of pixel values to that of 2D X-ray images from a commercially available adult anthropomorphic phantom. Data from the experiments included within our work provides evidence that the newly constructed phantom is valid for general X-ray imaging and optimisation studies. Furthermore, the face validity test showed that the phantom can be used with an IQ scale and this has valid performance for assessing of visual image quality (Cronbach's alpha coefficient about 0.8). This provides an additional indication that the phantom is fit for purpose, in terms of the visual assessment of IQ. In terms of accessibility, materials used within this phantom are widely available and come at relatively low cost, this makes manufacture simple. Manufacturing uses CT data which are, also, readily available and do not require specialist skills to undertake. Summarising all of the validation tests, this indicates that the phantom is valid for optimisation purposes and can be made from low cost materials, is relatively simply to construct and is likely to have global utility in areas with limited financial resources and access to phantoms.

Conflict of interest
We have no conflicts of interest to declare.

References

[1]   A. Jones, T. Simon, W. Bolch, M. Holman, D. Hintenlang, Tomographic physical phantom of the newborn child with real-time dosimetry I. Methods and techniques for construction, Med. Phys. 33 (2006). doi:10.1118/1.2256686.

[2]   Y. Watanabe, C. Constantinou, Phantom Materials in Radiology, in: Encycl. Med. Devices Instrum., John Wiley & Sons, Inc., Hoboken, NJ, USA, 2006: pp. 252–269. doi:10.1002/0471732877.emd201.

[3]   International Commission on Radiation Units and Measurements (ICRU), Phantoms

and Computational Models in Therapy, Diagnosis and Protection, Bethesda, Maryland, 1992. https://academic.oup.com/jicru/article/2923832/1.

[4] B.J. Conway, P.F. Butler, J.E. Duff, T.R. Fewell, R.E. Gross, R.J. Jennings, G.H. Koustenis, J.L. McCrohan, F.G. Rueter, C.K. Showalter, Beam quality independent attenuation phantom for estimating patient exposure from x-ray automatic exposure controlled chest examinations., Med. Phys. 11 (1984) 827–32. doi:10.1118/1.595611.

[5] J. Vassileva, A phantom for dose-image quality optimization in chest radiography, Br. J. Radiol. 75 (2002) 837–842. doi:10.1259/bjr.75.898.750837.

[6] V. Varchena, Pediatric phantoms, Pediatr. Radiol. 32 (2002) 280–284. doi:10.1007/s00247-002-0681-z.

[7] D. Hart, M. Hillier, B. Wall, Doses to Patients from Radiographic and Fluoroscopic X-ray Imaging Procedures in the UK – 2010 Review, 2007. http://www.hpa.org.uk/Publications/Radiation/CRCEScientificAndTechnicalReportSeries/HPACRCE034.

[8] C.G. Orton, ed., Progress in Medical Radiation Physics, Springer US, Boston, MA, 1982. doi:10.1007/978-1-4615-7691-4.

[9] F.E. Stieve, Radiological requirements for the specification of image quality criteria, Optim. Image Qual. Patient Expo. Diagnostic Radiol. BIR Report, 20. (1989) 221–238.

[10] A. Jones, Dose Versus Image Quality in Pediatric Radiology: Studies Using a Tomographic Newborn Physical Phantom with an Incorporated Dosimetry System, University of Florida, 2006. http://arxiv.org/abs/1011.1669.

[11] M.W. Bower, A Physical Anthropomorphic Phantom of a One-Year-Old Child with Real-Time Dosimetry, University of Florida, 1997.

[12] V. Varchenya, D. Gubatova, V. Sidorin, S. Kalnitsky, Children's Heterogeneous Phantoms and Their Application in Röntgenology, Radiat. Prot. Dosimetry. 49 (1993) 77–78. doi:10.1093/rpd/49.1-3.77.

[13] J.F. Winslow, D.E. Hyer, R.F. Fisher, C.J. Tien, D.E. Hintenlang, Construction of anthropomorphic phantoms for use in dosimetry studies, J. Appl. Clin. Med. Phys. 10 (2009) 195–204. doi:10.1120/jacmp.v10i3.2986.

[14] D.R. Pina, S.B. Duarte, T. Ghilardi Netto, C.S. Trad, M.A. Brochi, S.C. de Oliveira, Optimization of standard patient radiographic images for chest, skull and pelvis exams in conventional x-ray equipment, Phys. Med. Biol. 49 (2004) N215–N226. doi:10.1088/0031-9155/49/14/N02.

[15] D.R. Pina, S.B. Duarte, T. Ghilardi Netto, J. Morceli, Phantom development for radiographic image optimization of chest, skull and pelvis examination for nonstandard patient, Appl. Radiat. Isot. 67 (2009) 61–69. doi:10.1016/j.apradiso.2008.07.018.

[16] A.F.F. Alves, J.R.A. Miranda, F.A.B. Neto, S.B. Duarte, D.R. Pina, Construction of pediatric homogeneous phantoms for optimization of chest and skull radiographs, Eur. J. Radiol. 84 (2015) 1579–1585. doi:10.1016/j.ejrad.2015.05.015.

[17] K. Harrison, M. Ebert, T. Kron, S. Howlett, D. Cornes, C. Hamilton, J. Denham, Design, manufacture, and evaluation of an anthropomorphic pelvic phantom purpose-built for radiotherapy dosimetric intercomparison, Med. Phys. 38 (2011) 5330–5337. doi:10.1118/1.3626573.

[18] B.R. Paliwal, M.A. Ritter, T.R. McNutt, T.R. Mackie, B.R. Thomadsen, J.A. Purdy, T.J. Kinsella, A solid water pelvic and prostate phantom for imaging, volume rendering, treatment planning, and dosimetry for an RTOG multi-institutional, 3-D dose escalation study, Int. J. Radiat. Oncol. Biol. Phys. 42 (1998) 205–211. doi:10.1016/S0360-3016(98)00187-4.

[19] L. Duggan, H. Warren-Forward, T. Smith, T. Kron, Investigation of dose reduction in neonatal radiography using specially designed phantoms and LiF:Mg,Cu,P TLDs, Br. J. Radiol. 76 (2003) 232–237. doi:10.1259/bjr/79291075.

[20] E. Nickoloff, Current adult and pediatric CT doses, Pediatr. Radiol. 32 (2002) 250–260. doi:10.1007/s00247-002-0677-8.

[21] G. Giacco, V. Cannata, C. Furetta, F. Santopietro, G. Fariello, On the use of pediatric phantoms in the dose evaluation during computed tomography (CT) thorax examinations, Med. Phys. 28 (2001) 199. doi:10.1118/1.1344205.

[22] D.R. Pina, Metodologia para otimização de imagems radiográfica, University of Sao Paulo, USP, Brazil, 2002.

[23] B. Schaly, V. Varchena, P. Au, G. Pang, Evaluation of an anthropomorphic male pelvic phantom for image-guided radiotherapy, Reports Med. Imaging. (2009) 69–78. http://www.dovepress.com/getfile.php?fileID=5090.

[24] J.H. Hubbell, Tables of X-Ray Mass Attenuation Coefficients and Mass Energy-Absorption Coefficients from 1 keV to 20 MeV for Elements Z = 1 to 92 and 48 Additional Substances of Dosimetric Interest, NISTIR 5632. Natl Inst Stand. Technol, USA. (1995). http://www.nist.gov/pml/data/xraycoef/ (accessed January 25, 2016).

[25] International Commission on Radiation Units and Measurements (ICRU), Tissue substitutes in radiation dosimetry and measurement, Bethesda, Maryland, 1989.

[26] S.P. Knight, A paediatric X-ray exposure chart, J. Med. Radiat. Sci. 61 (2014) 191–201. doi:10.1002/jmrs.56.

[27] M. Goitein, Applications of Computed Tomography in Radiotherapy Treatment Planning, in: Prog. Med. Radiat. Phys., Springer US, Boston, MA, 1982: pp. 195–293. doi:10.1007/978-1-4615-7691-4_4.

[28] D. White, The formulation of substitute materials with predetrmined characteristics of radiation absorption and scattering, Queen Mary, University of London, 1974.

[29] C.T.P. Chan, K.K.L. Fung, Dose optimization in pelvic radiography by air gap method on CR and DR systems – A phantom study, Radiography. 21 (2015) 214–223. doi:10.1016/j.radi.2014.11.005.

[30] N. Sheridan, J.P. McNulty, Computed radiography versus indirect digital radiography for the detection of glass soft-tissue foreign bodies, Radiography. 22 (2016) 223–227. doi:10.1016/j.radi.2016.02.003.

[31] S. Mattsson, B. Thomas, Development of methods for body composition studies, Phys. Med. Biol. Phys. Med. Biol. 51 (2006) 203–228. doi:10.1088/0031-9155/51/13/R13.

[32] P. Homolka, R. Nowotny, Production of phantom materials using polymer powder sintering under vacuum., Phys. Med. Biol. 47 (2002) N47-52. http://www.ncbi.nlm.nih.gov/pubmed/11848127.

[33] T.L. Fauber, Radiographic Imaging and Exposure, 4th ed., Elsevier Health Sciences, 2013.

[34] R. Bourne, Fundamentals of Digital Imaging in Medicine, Springer London, London, 2010. doi:10.1007/978-1-84882-087-6.

[35] E. Samei, N.T. Ranger, A. MacKenzie, I.D. Honey, J.T. Dobbins, C.E. Ravin, Effective DQE (eDQE) and speed of digital radiographic systems: an experimental methodology., Med. Phys. 36 (2009) 3806–3817. doi:10.1118/1.3171690.

[36] M. Sandborg, A. Tingberg, G. Ullman, D. Dance, G. Carlsson, Comparison of clinical and physical measures of image quality in chest and pelvis computed radiography at different tube voltages, Med. Phys. 33 (2006) 4169–4175. doi:10.1118/1.2362871.

[37] H. Mraity, A. England, S. Cassidy, P. Eachus, A. Dominguez, P. Hogg, Development and validation of a visual grading scale for assessing image quality of AP pelvis radiographic images, Br. J. Radiol. 89 (2016) 20150430. doi:10.1259/bjr.20150430.

[38] A. Tingberg, C. Herrmann, B. Lanhede, A. Almén, M. Sandborg, G. McVey, S. Mattsson, W. Panzer, J. Besjakov, L.G. Månsson, S. Kheddache, G. Alm Carlsson, D.R. Dance, U. Tylén, M. Zankl, Influence of the characteristic curve on the clinical image quality of lumbar spine and chest radiographs, Br. J. Radiol. 77 (2004) 204–215. doi:10.1259/bjr/22642890.

[39] L. Lança, L. Franco, A. Ahmed, M. Harderwijk, C. Marti, S. Nasir, J. Ndlovu, M. Oliveira, A.R. Santiago, P. Hogg, 10kVp rule - An anthropomorphic pelvis phantom imaging study using a CR system: Impact on image quality and effective dose using AEC and manual mode, Radiography. 20 (2014) 333–338. doi:10.1016/j.radi.2014.04.007.

[40] D. White, C. Constantinou, Anthropomorphic Phantom Materials, in: Prog. Med. Radiat. Phys., Springer US, Boston, MA, 1982: pp. 133–193. doi:10.1007/978-1-4615-7691-4_3.

[41] S. Leng, K. McGee, J. Morris, A. Alexander, J. Kuhlmann, T. Vrieze, C.H. McCollough, J. Matsumoto, Anatomic modeling using 3D printing: quality assurance and optimization, 3D Print. Med. 3 (2017) 6. doi:10.1186/s41205-017-0014-3.

[42] S. Leng, L. Yu, T. Vrieze, J. Kuhlmann, B. Chen, C.H. McCollough, Construction of realistic liver phantoms from patient images using 3D printer and its application in CT image quality assessment, in: C. Hoeschen, D. Kontos, T.G. Flohr (Eds.), HHS Public Access, 2015: p. 94124E. doi:10.1117/12.2082121.
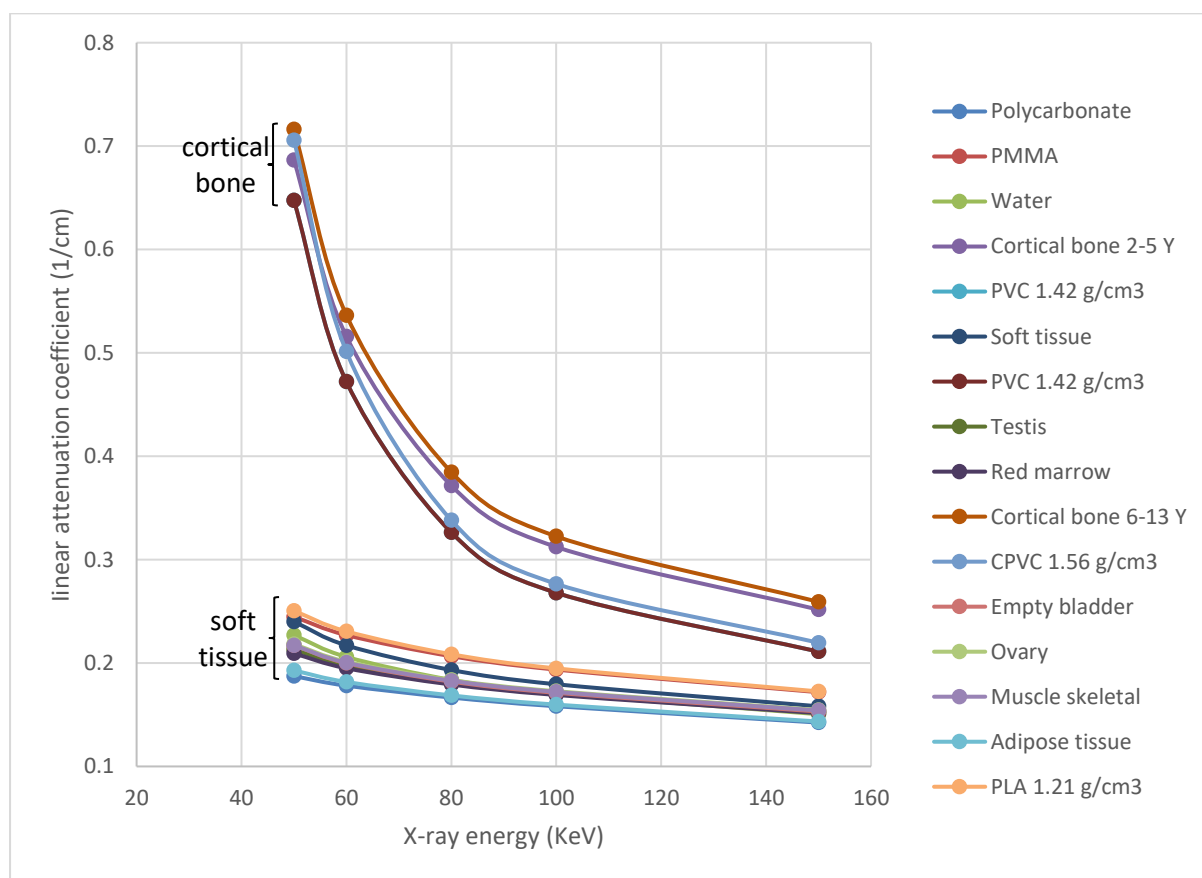
Figures and Tables with their Descriptions

Figure 1. Linear attenuation coefficients for different human tissues, organs and substitutes.
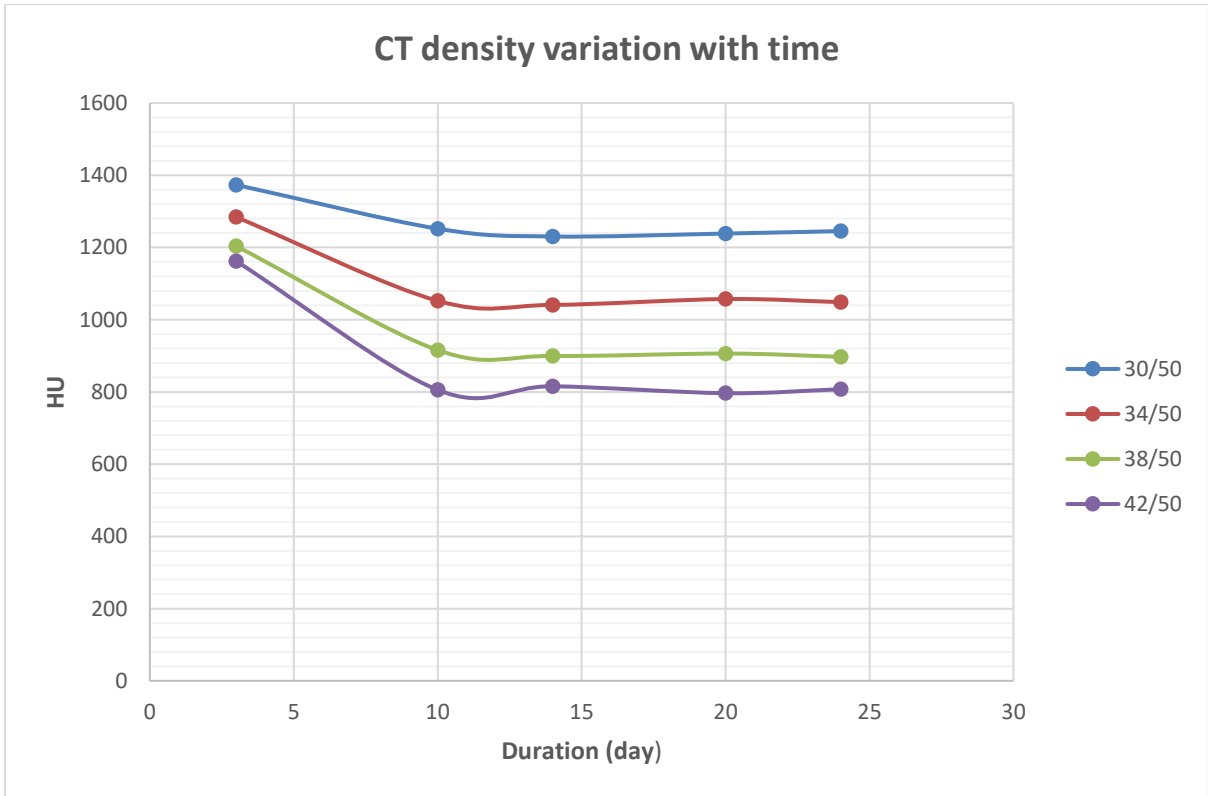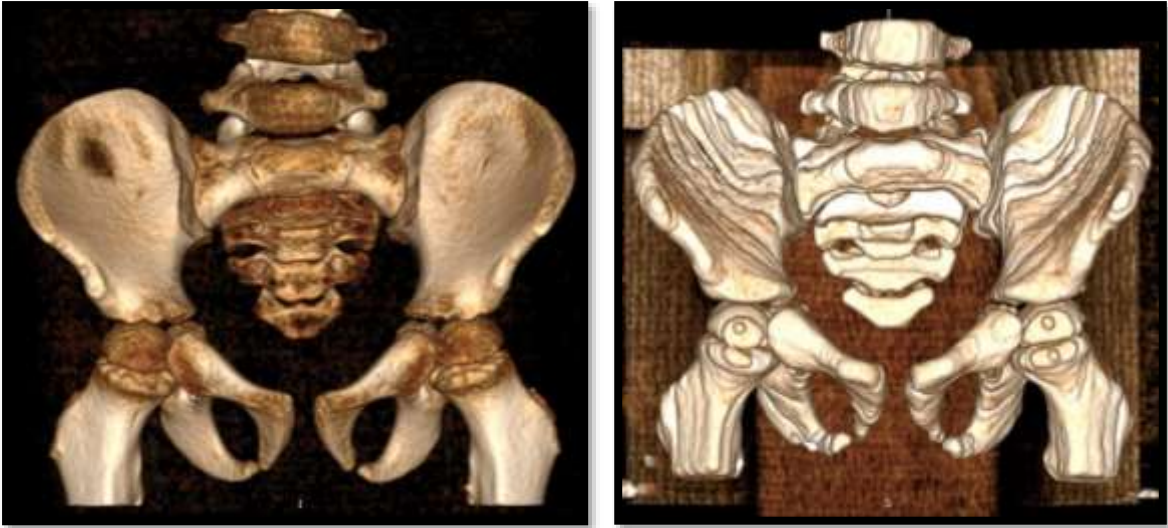
Figure 2: Time changes in CT density for the different PoP weight-mixing ratios.

Figure 3. Adjacent PMMA slices, within the PMMA slices are the bony anatomical cavities ready for filling with PoP.

<center>(a)   (b)</center>

Figure 4. AP pelvic volume rendered CT image of (a) the real patient and (b) the phantom.

<center>(a)   (b)</center>

Figure 5. ROI sizes and measurement locations on the (a) our 5-year-old (new) phantom and (b) the adult phantom.

<center>**Table (1)**: Comparison of CT density for the phantom materials versus human patient tissue.</center>

Material	**Mean HU (SD range)**	**Percentage difference**
PoP	1249.9(50.2-135.5) to 1258.4(46.1-137.0)	-4.7 to -4.1%
Cortical bone	1200.2 (111.5-297.3)	
Animal bone	1212.4 (111.4-280.7)	-1.0%
Cortical bone	1200.2 (111.5-297.3)	

Soft tissue	74.0 (20.7-25.4)	-23.4%
PMMA	93.6 (35.2-57.9)	
Cortical bone	1200.2 (111.5-297.3)	176.8%
Soft tissue	74.0 (20.7-25.4)	
Averaged PoP	1255.3	172.2%
PMMA	93.6 (35.2-57.9)	

PoP, Plaster of Paris; HU, Hounsfield unit; SD, standard deviation; min, minimum; max, maximum.

Table (2): Correlation between the pixel value data from adult and 5-year old child phantom. The 5-year old (new) phantom had a thickness (21 cm) matching the adult phantom.

Correlation coefficient					
Response to changing mAs			**Response to changing kVp**		
Adult vs. 5-year old			Adult vs 5-year old		
kVp	PMMA	ROIs	mAs	PMMA	ROIs
50	0.995	0.994	1	0.981	0.974
53	0.982	0.983	2	0.947	0.921
56	0.988	0.987	2.8	0.931	0.891
59	0.995	0.995	4	0.904	0.818
62	0.99	0.99	5	0.885	0.789
65	0.992	0.992	6.3	0.863	0.724
68	0.996	0.996	7.1	0.842	0.648
71	0.993	0.992	8	0.822	0.582
74	0.995	0.995	9	0.795	0.492
77	0.991	0.991	10	0.757	0.352
80	0.987	0.987	11	0.735	0.3
83	0.989	0.989	12.5	0.715	0.135
86	0.979	0.978	14	0.675	-0.41
89	0.955	0.953	16	0.645	-0.175
92	0.982	0.981	18	0.575	-0.445
95	0.973	0.971	20	0.394	-0.811
98	0.978	0.978			
101	0.979	0.979			

All correlations reported in the table were statistically significant ($p<0.05$). With respect to the 'response to changing mAs' data, for each kVp a number of mAs values were tested and thus generated the correlation coefficients for PMMA and bone. This was also similar for the 'response to changing kVp' where for each mAs value there were a number of acquisitions obtained at different kVps resulting in a correlation coefficient for PMMA and bone.

Table (3): Average score answers for the face validity questions.

	Q1	Q2	Q3	Q4	Q5	Q6	Q7	Q8	Q9	Q10	Q11	Q12	Q13	Q14	Q15
Average score	0.88	0.03	0.84	0.39	0.55	0.34	0.53	0.52	0.53	0.03	0.75	0.13	0.68	0.35	0.84
SD	0.61	1.00	0.63	0.95	0.89	0.90	0.97	0.96	0.86	1.07	0.80	0.94	0.79	0.91	0.92

Average (Q1-Q14)	0.47